Optics Letters

Dynamic computer-generated nonlinear optical holograms in a non-collinear second-harmonic generation process

Haigang Liu,[1,2] Xiaohui Zhao,[3] Hui Li,[1,2] Yuanlin Zheng,[1,2,4] and Xianfeng Chen[1,2,5]

[1]State Key Laboratory of Advanced Optical Communication Systems and Networks, School of Physics and Astronomy, Shanghai Jiao Tong University, Shanghai 200240, China
[2]Key Laboratory for Laser Plasma (Ministry of Education), Collaborative Innovation Center of IFSA (CICIFSA), Shanghai Jiao Tong University, Shanghai 200240, China
[3]Shanghai Institute of Laser Plasma, Shanghai 201800, China
[4]e-mail: ylzheng@sjtu.edu.cn
[5]e-mail: xfchen@sjtu.edu.cn

Received 30 April 2018; revised 6 June 2018; accepted 8 June 2018; posted 11 June 2018 (Doc. ID 330633); published 5 July 2018

The nonlinear holography technique is a powerful tool for all-optical switching and manipulation of an arbitrary harmonic wave. The common method of realizing such nonlinear holography is by configuring the structure of nonlinear photonic crystals. However, it is a challenge to dynamically tune the harmonic wave pattern. To overcome the long-term existing non-dynamic property of such nonlinear holographs, we realize dynamic computer-generated nonlinear optical holograms in the non-collinear second-harmonic (SH) generation process in which only one infrared beam is modulated. Arbitrary patterns in both fundamental-frequency and second-harmonic wavebands can be generated at the same time. This Letter offers a flexible and dynamic method for arbitrary nonlinear wavefront shaping technology.

OCIS codes: (190.0190) Nonlinear optics; (090.1760) Computer holography; (050.1970) Diffractive optics; (190.2620) Harmonic generation and mixing.

https://doi.org/10.1364/OL.43.003236

The holography technique, which records and reconstructs the amplitude and phase of a wave from an illuminated object, has been developed for decades. It has been widely used in various fields, such as hologram optical tweezing [1,2], micro-fabrication [3,4], and optical communication [5,6]. With the coming of the digital age, the combination of holography and the digital processing technology led to the emergence of a computer-generated hologram (CGH). It is the key step to realize the real sense of dynamic holography display, which is the most desired in the future. In recent years, the nonlinear holography technique plays a more and more important role in areas of nonlinear optics and hologram display due to its capability of the potential applications in all-optical switching and manipulation of the generated electromagnetic wave. One of the most important applications of such a nonlinear holography technique is shaping the nonlinear harmonic wavefront in a nonlinear conversion process. The common method of realizing such nonlinear wavefront shaping is by tailoring the size and spatial structure of nonlinear photonic crystals (NPCs) [7–19]. The holography concept is introduced to the nonlinear field by shaping the nonlinear light wave along the quasi-phase-matching direction in a one-dimensional manner [8]. After that, two-dimensional (2D) SH beam shaping is achieved along the transverse direction of a binary modulated NPC [9,10]. Besides, nonlinear volume holography has also been proposed and realized in recent years [11,12]. However, all these works possess the same problem, i.e., the non-dynamic property of the nonlinear harmonic wave and complex manufacture of the nonlinear sample. Hence, in nonlinear optics, finding a flexible and dynamic method to realize the same function of nonlinear harmonic wave conversion and the holography technique is of significant importance in areas of nonlinear optics and hologram display industry.

Recent studies show that such a non-dynamic property of the nonlinear harmonic wave can be solved by dynamically controlling the incident fundamental-frequency wave [20]. We also proposed the concept of dynamic computer-generated nonlinear optical holograms [21]. In this Letter, the latest progress of the realization of such dynamic computer-generated nonlinear optical holograms in the non-collinear second-harmonic (SH) process is reported. By using this method, arbitrary patterns in both fundamental-frequency and SH wavebands can be reconstructed at the same time. In our experiment, the letters of "A" and "B" can be well reconstructed. To demonstrate the reconstruction ability of this method, a more complex pattern and an image of the continuously changing amplitude are realized. We also analyze the influence factors of the quality of the reconstructed image. Finally, a movie of a running horse is realized to show the dynamic property of this method.

Suppose that the object wave propagates along the z-axis in the process of a CGH, a spatial light modulator (SLM) can be used to generate the interference pattern of a reference

wave $R = A\exp(-j2\pi\alpha y)$ and an object wave $O(x,y) = O_0(x,y)\exp[-j\phi(x,y)]$, where α is the angle between them. When a plane wave with amplitude C is incident onto the SLM, the reconstructed light wave can be expressed as

$$U(x,y) = Ct_b + \beta'[|O(x,y)|^2 C + \mathrm{CAO}\exp(j2\pi\alpha y) + \mathrm{CAO}^*\exp(-j2\pi\alpha y)], \quad (1)$$

where t_b is the transmittance of the SLM, and β' is a constant. The second and last terms can be removed by using a spatial filter (SF). Hence, only a plane wave $E_R(\omega) = Ct_b$ and an object wave $E_O(\omega) = \mathrm{CAO}\exp(j2\pi\alpha y)$ are incident into a nonlinear crystal with an angle α, which can be dynamically controlled by the computation process. A dynamic nonlinear grating would be generated when $E_R(\omega)$ and $E_O(\omega)$ meet each other in the nonlinear crystal.

In the process of second-harmonic generation (SHG), by utilizing the principle of the nonlinear holograph [11,12], the nonlinear polarization wave $E_{\mathrm{NPW}}(2\omega) = [\chi^{(2)}/\chi^{(1)}]E_R(\omega)E_O(\omega)$ is treated as the reference beam to interfere with the SH wave (SHW) $E_{\mathrm{SHW}}(2\omega)$. Here $\chi^{(1)}$ and $\chi^{(2)}$, respectively, are the linear and second-order nonlinear optical susceptibility, and $E_R(\omega)$ and $E_O(\omega)$ are the incident fundamental waves (FWs). The structure of $\chi^{(2)}$ in the nonlinear crystal or the incidental FW can be given by the following expression:

$$f(x,y,z) = E^*_{\mathrm{SHW}}E_{\mathrm{NPW}} + E_{\mathrm{SHW}}E^*_{\mathrm{NPW}}, \quad (2)$$

where $f(x,y,z)$ denotes the modulated structure function of the FW or the NPC. In the case of a modulated nonlinear crystal ($\chi^{(2)}$ modulation), $f(x,y,z)$ needs to be binary, which is determined by the property of the nonlinear crystals. In most ferroelectric crystals, such $\chi^{(2)}$ modulation is along the c-axis, which limits the modulating property of the SH. Unlike $\chi^{(2)}$ modulation, we focus on the structure property in the incidental FW, which can be dynamically controlled in the CGH process.

To get arbitrary shapes of SH in the far field, the Fourier electric field of the object is recorded. The Fourier transform relation between the far field and near field can be expressed as

$$E(x_1,y_1) = \frac{e^{jkz}}{j\lambda_{\mathrm{SH}}z}e^{j\frac{k}{2z}(x_1^2+y_1^2)}\mathcal{F}\left\{E(x,y)e^{j\frac{k}{2z}(x^2+y^2)}\right\}_{f_x=\frac{x}{\lambda_{\mathrm{SH}}z},\,f_y=\frac{y}{\lambda_{\mathrm{SH}}z}}, \quad (3)$$

where x,y,z and x_1,y_1, respectively, are the coordinates at planes of Σ and Σ_1, depicted in Fig. 1; λ_{SH} and k, respectively, are the wavelength and wavevector of the SHW; f_x and f_y, respectively, are the spatial frequency of the SHW along x and y direction; and $E(x_1,y_1)$ and $E(x,y)$, respectively, represent the amplitudes of SHW at plane Σ and Σ_1.

The schematic of the experimental setup is shown in Fig. 1(a). The FW is delivered from an Nd:YAG nanosecond laser, and the wavelength is 1064 nm. The laser produces 4 ns pulses, and the repetition rate is 20 Hz. A half-wave plate and a polarization beam splitter are used to control the polarization and intensity of the FW [not shown in Fig. 1(a)]. The SLM has a resolution of 512×512 pixels, each with a rectangular area of $19.5\times19.5\ \mu\mathrm{m}^2$. After passing through the SLM, the FW is imaged by a $4-f$ system, composed of lens $L_1(f_1 = 200\ \mathrm{mm})$ and $L_2(f_2 = 50\ \mathrm{mm})$, to imprint the modulated wavefront pattern onto the onset of a $\chi^{(2)}$ crystal.

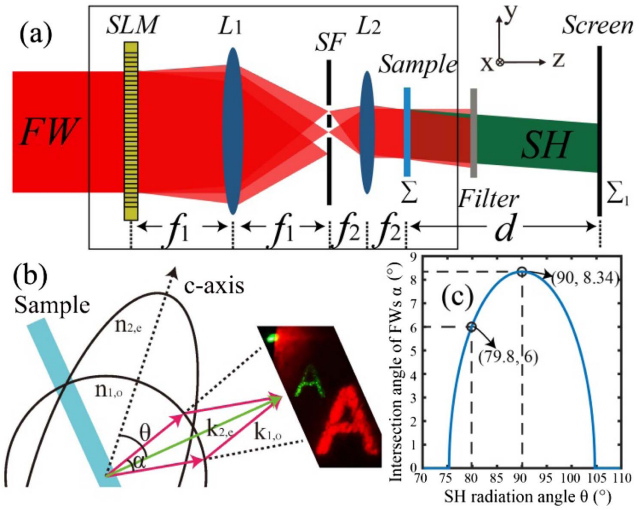

Fig. 1. (a) Schematic of the experimental setup to realize arbitrary shapes of SHG. SLM, spatial light modulator; $L_{1\text{–}2}$, lens, $f_{1\text{–}2} = 200$ and 50 mm, respectively; SF, spatial filter; sample, 5 mol. % MgO, $LiNbO_3$. (b) Phase-matching diagram of the non-collinear SHG process. (c) Relation between SH radiation angle θ and the intersection angle of FWs α.

An SF is used to filter out undesired FW after the SLM. The beam waist is about 2 mm at the onset of the nonlinear crystal. After the crystal, a short-pass filter is used to filter out the FW. Finally, the generated SH beam is projected on a screen in the far-field ($d = 30$ cm) and recorded by a camera. For simplicity and without the loss of generality, the sample of a 5 mol. % MgO:$LiNbO_3$ thin bulk crystal is used (0.5 mm thick). Figure 1(b) shows the phase-matching diagram of the non-collinear SHG process. The FW is kept as o-polarized, and the generated SH is e-polarized. In a non-collinear SHG process, the intersection angle α of such two fundamental-frequency waves, in which the wavevector located on two sides of the birefringent phase-matching direction, is 6°. Rotating nonlinear crystal to find the phase-matching point, in which n_{2e} is slightly smaller than n_{1o}. In our experiment, SH radiation angle θ is 79.8° with respect to the c-axis of $LiNbO_3$ crystal. The birefringent phase-matching angle is 75° according to the Sellmeier equation in [22]. According to the relation between θ and α shown in Fig. 1(c), to keep phase-matching condition, the intersection angle of such two fundamental-frequency waves should smaller than 8.34°.

Such a method allows for arbitrary pattern generation in both fundamental-frequency and SH wavebands. First, the letters of "A" and "B" are realized, as shown in Fig. 2. The desired SH patterns are shown in Figs. 2(a) and 2(e). It should be noticed that, in order to lower the dynamic variation range of the Fourier spectrum of the desired SH pattern, a random phase is added in the process of phase structure design. The corresponding holographic phase structures of the FW are shown in Figs. 2(b) and 2(f). Figures 2(c) and 2(g) show the corresponding experimental result of the SH images. Removing the short-pass filter shown in Fig. 1(a), a NIR sensor card is used to convert the fundamental-frequency light at 1064 nm to the visible red light. Figures 2(d) and 2(h) show the

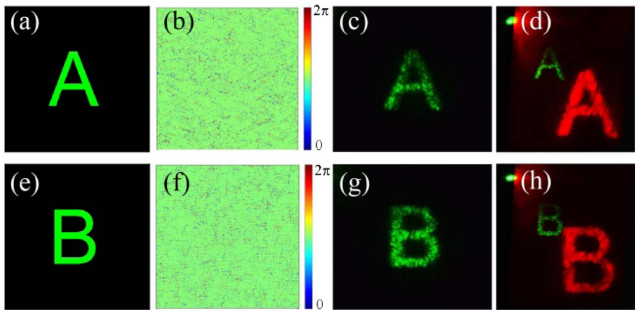

Fig. 2. (a) and (e) Profiles of the desired SH patterns correspond to letter "A" and "B," respectively. (b) and (f) Holographic phase structures of the FW correspond to (a) and (e), respectively. (c) and (g) Experimentally reconstructed SH patterns in the far field. (d) and (h) Experimentally reconstructed holographic patterns in both fundamental-frequency and SH wavebands in the far field.

generated holographic pattern in both fundamental-frequency and SH wavebands. Compared with the pattern in fundamental frequency, the smaller of the SH holographic pattern is caused by the longer wavevector of the SH. The experimental results agree well with the desired pattern.

It should be pointed out that the phase structure of the FW could vary from 0 to 2π, which also means the phase of the SH can almost be continually changed. This property cannot be realized in the method of manipulating the structure of the NPCs. Domain reversal of the NPCs is only along the z-axis. Hence, in previous 2D SH shaping, the FW only propagates along the c-axis, which limit the nonlinear conversion efficiency of the SH. However, the structured FW can propagate along nearly arbitrary direction of the nonlinear crystal. In [21], we have shown that the conversion efficiency of the double-frequency process could dramatically increase by utilizing the method of modulating the FW. The non-collinear SHG process is also a phase-matched SH process, hence it also could have high conversion efficiency. In our experiment, the energy of one input fundamental light is about 1 mJ and the energy of the generated SH is 2.5 μJ. The conversion efficiency for peak power is about $1 \times 10^{-6}\%\ \mathrm{W}^{-1}$. For a longer nonlinear crystal (0.5 mm in our experiment), the conversion efficiency would much higher. However, free-space holograms require an optically thin medium, which provide well-defined amplitude and phase plane. Hence, the longer nonlinear crystal would reduce the quality of the reconstructed image.

Although some simple pattern can be relatively well reconstructed by this method, a more interesting case is to study the quality of a complex SH image, which is shown in Fig. 3 (holographic patterns at fundamental frequency are not shown hereafter). Figure 3(a) is the desired SH amplitude pattern. The experimental result is shown in Fig. 3(b) and most of the property of the desired SH is realized. However, the detail of the pattern, such as the numbers in the pattern, cannot be reconstructed. In the experiment, the fundamental light with phase modulation is treated as the paraxial beam. In fact, the quality of reconstructed image is influenced by the diffraction of fundamental light in the actual situation. The details of a complex image [the numbers in the pattern of Fig. 3(a)] correspond to the large spatial frequency, which may break the phase-matching condition of the SHG process. Hence, the

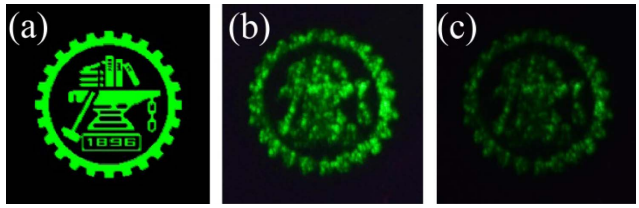

Fig. 3. (a) Profiles of a more complex SH pattern. (b) Experimentally generated SH pattern in the far field corresponding to (a). (c) Experimentally reconstructed SH pattern in the far field when half of the SLM is blocked.

detail of the pattern in Fig. 3(a) is not reconstructed. Another reason may lie in the record process. For a complex image, the number of the SLM pixels is not enough to reconstruct the image of more details. Next, an aperture is used to block half of the SLM. In this case, the SH can also be reconstructed except for relatively low intensity, as shown in Fig. 3(c). This is an important property of the holograph, in which the information of the object is recorded on each element of the hologram image.

Next, SH with a continuously changing amplitude is analyzed, as shown in Fig. 4. Figures 4(a) and 4(b) are the desired SH pattern and the corresponding experimental result, respectively. The comparison of transverse profile of the SH intensity is shown in Fig. 4(c). It indicates that the overall intensity of the experimental result and the desired SH pattern is consistent with each other despite the intensity fluctuation in the cross section. That is because of the phase randomness factor in the of a CGH process.

To illustrate the dynamic property of such method, a dynamic running horse is also realized, as shown in Fig. 5. The first and third rows of Fig. 5 are the profiles of the SH patterns corresponding to different time frames of a running horse. The second and fourth rows are the corresponding experimentally generated SH patterns. The dynamic property is mainly determined by the SLM, whose responding time is on the order of hundreds of micro-seconds. In our experiment, an Nd:YAG nanosecond laser with the repetition rate of 20 Hz is used. Hence, the refresh rate of the SLM is reduced to match that of the laser. The video of the dynamic running horse in both fundamental frequency and SH waveband is shown in Visualization 1.

The relationship between the holograph and the non-collinear SH has been investigated [23,24]. However, they need complex arrangement of optical components. The key difference of our method as compared with previous researches

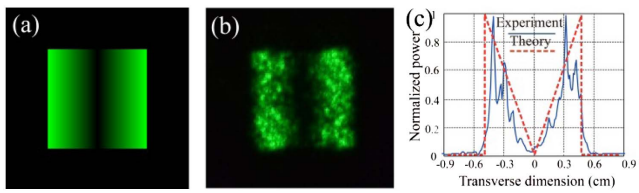

Fig. 4. (a) Profile of an SH pattern with a continually varying amplitude. (b) Generated SH pattern in the experiment. (c) Cross section of the simulated (solid red curve) and measured (dashed blue curve) intensities of the SH.

Fig. 5. First and third rows are the profiles of the SH patterns corresponding to different times of a running horse. The second and fourth rows are the profiles of the experimentally generated SH patterns corresponding to the first and third rows. The video of the dynamic running horse in both fundamental-frequency and SH wavebands is shown in Visualization 1.

is that we combine the CGH with non-collinear SHG. Such a CGH can be used to generate arbitrary pattern theoretically. In [23,24], the angle and overlap of the mode in different optical beams need to be carefully arranged. However, these problems can be solved by the computed process and a simple $4-f$ system, respectively. The combination of the CGH and the non-collinear SHG process is a more flexible way to realize arbitrary SH shaping. The combination of the dynamic CGH and the nonlinear process is expected to play a critical role in the holographic display industry by providing an effective pathway of dynamic all-optical switching and manipulation of arbitrary nonlinear harmonic wave holographic images.

In conclusion, we realized the dynamic computer-generated nonlinear optical holograms in a non-collinear SH process. In our experiment, various arbitrary shapes of SH patterns are generated. Besides, we also carefully analyzed the factor of influence of the quality of the constructed SH pattern, including complexity and continuous characteristic of the generated SH pattern. Compared with previous nonlinear holograms, this method does not need a complex arrangement of optical components and fabrication of the NPCs. Hence, this Letter offers a flexible and dynamic method for arbitrary nonlinear wavefront shaping technology.

Funding. National Key R&D Program of China (2017YFA0303700); National Natural Science Foundation of China (NSFC) (11734011); The Foundation for Development of Science and Technology of Shanghai (17JC1400400).

REFERENCES

1. A. N. Grigorenko, N. W. Roberts, M. R. Dickinson, and Y. Zhang, Nat. Photonics **2**, 365 (2008).
2. E. R. Dufresne, G. C. Spalding, M. T. Dearing, S. A. Sheets, and D. G. Grier, Rev. Sci. Instrum. **72**, 1810 (2001).
3. W. Gao, N. Singh, L. Song, Z. Liu, A. L. M. Reddy, L. J. Ci, R. Vajtai, Q. Zhang, B. Q. Wei, and P. M. Ajayan, Nat. Nanotechnol. **6**, 496 (2011).
4. J. Lin, Y. Xu, Z. Fang, M. Wang, J. Song, N. Wang, L. Qiao, W. Fang, and Y. Cheng, Sci. Rep. **5**, 8072 (2015).
5. J. Wang, J. Y. Yang, I. M. Fazal, N. Ahmed, Y. Yan, H. Huang, Y. X. Ren, Y. Yue, S. Dolinar, M. Tur, and A. E. Willner, Nat. Photonics **6**, 488 (2012).
6. J. Chu, X. Li, Q. Smithwick, and D. Chu, Opt. Lett. **41**, 1490 (2016).
7. T. Ellenbogen, N. Voloch-Bloch, A. Ganany-Padowicz, and A. Arie, Nat. Photonics **3**, 395 (2009).
8. A. Shapira, I. Juwiler, and A. Arie, Opt. Lett. **36**, 3015 (2011).
9. N. V. Bloch, K. Shemer, A. Shapira, R. Shiloh, I. Juwiler, and A. Arie, Phys. Rev. Lett. **108**, 233902 (2012).
10. A. Shapira, R. Shiloh, I. Juwiler, and A. Arie, Opt. Lett. **37**, 2136 (2012).
11. X. H. Hong, B. Yang, C. Zhang, Y. Q. Qin, and Y. Y. Zhu, Phys. Rev. Lett. **113**, 163902 (2014).
12. B. Yang, X. H. Hong, R. E. Lu, Y. Y. Yue, C. Zhang, Y. Q. Qin, and Y. Y. Zhu, Opt. Lett. **41**, 2927 (2016).
13. S. Trajtenberg-Mills, I. Juwiler, and A. Arie, Laser Photon. Rev. **9**, L40 (2015).
14. A. Shapira, I. Juwiler, and A. Arie, Laser Photon. Rev. **7**, L25 (2013).
15. S. Lightman, R. Gvishi, G. Hurvitz, and A. Arie, Opt. Lett. **40**, 4460 (2015).
16. A. Shapira, L. Naor, and A. Arie, Sci. Bull. **60**, 1403 (2015).
17. K. Shemer, N. Voloch-Bloch, A. Shapira, A. Libster, I. Juwiler, and A. Arie, Opt. Lett. **38**, 5470 (2013).
18. Y. Qin, C. Zhang, Y. Zhu, X. Hu, and G. Zhao, Phys. Rev. Lett. **100**, 063902 (2008).
19. T. Ellenbogen, I. Dolev, and A. Arie, Opt. Lett. **33**, 1207 (2008).
20. A. Libster-Hershko, S. Trajtenberg-Mills, and A. Arie, Opt. Lett. **40**, 1944 (2015).
21. H. Liu, J. Li, X. Fang, X. Zhao, Y. Zheng, and X. Chen, Phys. Rev. A **96**, 023801 (2017).
22. O. Gayer, Z. Sacks, E. Galun, and A. Arie, Appl. Phys. B **91**, 343 (2008).
23. A. Andreoni, M. Bondani, and M. A. C. Potenza, Opt. Lett. **25**, 1570 (2000).
24. Y. N. Denisyuk, A. Andreoni, M. Bondani, and M. A. C. Potenza, Opt. Lett. **25**, 890 (2000).